Measurement and properties of dose-area product ratio in external small-beam radiotherapy

Jarkko Niemelä[1,2], Mari Partanen[3,4], Jarkko Ojala[3,4], Petri Sipilä[5], Mikko Björkqvist [1,2], Mika Kapanen[3,4], Jani Keyriläinen[1,2]

[1]Department of Medical Physics, Division of Expert services, Turku University Hospital, P.O.Box 52, FI-20521 Turku, Finland

[2]Department of Oncology and Radiotherapy, Turku University Hospital, P.O.Box 52, FI-20521 Turku, Finland

[3]Department of Oncology, Unit of Radiotherapy, Tampere University Hospital, P.O. Box 2000, FI-33521 Tampere, Finland

[4]Department of Medical Physics, Tampere University Hospital, P.O. Box 2000, FI-33521 Tampere, Finland

[5]Radiation Practices Regulation, Radiation in Health Care, STUK—Radiation and Nuclear Safety Authority, Helsinki, Finland

Abstract:

In small-beam radiation therapy (RT) the measurement of beam quality parameter i.e. tissue-phantom ratio or $TPR_{20,10}$ with conventional point detector is a challenge. To obtain reliable results, one has to consider potential sources of error, including volume averaging and adjustment of the point detector into the narrow beam. To overcome these challenges, a different type of possible beam quality parameter in small beams was studied, namely the dose-area product ratio or $DAPR_{20,10}$. With this method, the measurement of a dose-area product (DAP) with a large-area plane-parallel chamber (LAC) eliminates the uncertainties in detector positioning and volume averaging present with the use of a point detector. In this study, properties of $DAPR_{20,10}$ of cone-collimated 6 MV photon beam were investigated with Monte Carlo (MC) calculations and the obtained va lues were compared to measurements obtained by two LAC detectors PTW Type 34073 and PTW Type 34070. In addition, the possibility of determining the DAP with EBT3 film and Razor diode detector was studied. The determination of $DAPR_{20,10}$ value was found to be feasible in external small-beam radiotherapy of cone-collimated beams with diameters from 4 to 40 mm with the two LACs, MC calculation and Razor diode. Measurements indicated a constant $DAPR_{20,10}$ value for fields from 20 to 40 mm in diameter with maximum relative change of 0.6%, but an increase of 7.0% for fields from 20 to 4 mm in diameter for PTW Type 34070 chamber. Simulations and measurements showed an increase of $DAPR_{20,10}$ with increasing LAC size or dose integral area for studied cone-collimated 6 MV photon beams from 4 to 40 mm in diameter. This has a consequence that with reported $DAPR_{20,10}$ value there should be a reference to the size of the used LAC active area or the DAP integration area.

Measurement and properties of dose-area product ratio in external small-beam radiotherapy

Introduction

Small field sizes are increasingly used in external radiation therapy (RT). In stereotactic radiation surgery (SRS) of the brain and stereotactic body radiation therapy (SBRT) the size of a tumor may be only a few millimetres. In intensity modulated radiation therapy (IMRT) and volumetric modulated arc therapy (VMAT) techniques the beams are divided into small beamlets with a size of the order of a millimetre. In small-beam RT with beam diameter less than 2 cm there are several issues to consider, including the loss of lateral electronic equilibrium, partial radiation source occlusion, detector and beam placement uncertainty as well as volume averaging of detector signal (Li *et al* 1995, Das *et al* 2008, Alfonso *et al* 2008, Charles *et al* 2014, Benmakhlouf *et al* 2014). In order to overcome these issues, rather than determining the dose on the beam central axis (CAX) with point dose measurements, the dose could be measured in terms of dose-area product (DAP) (Djouguela *et al* 2006, Dufreneix *et al* 2016). Output factors (OFs) have been determined with DAP (Djouguela *et al* 2006, Sánchez-Doblado *et al* 2007) by measuring the ionisation through an area encompassing the whole beam and in right angles to the beam with a large-area plane-parallel ionisation chamber (LAC) in solid water. Also, the beam quality parameter, i.e. tissue-phantom-ratio at 20 and 10 cm depths ($TPR_{20,10}$) has been proposed to be replaced by dose-area-product ratio at 20 and 10 cm depths ($DAPR_{20,10}$) with a constant source-to-detector distance of 100 cm in small-beam RT.

In this study, the properties of two commercial LACs were investigated by measuring DAP and $DAPR_{20,10}$ in water for small cone-collimated photon beam with nominal energy of 6 MV ranging from 4 to 40 mm in diameter. In addition, the possibility of determining DAP in solid water phantom by means of film measurements was studied. In order to investigate the dependence of DAP and $DAPR_{20,10}$ on the dose measuring area and perturbations induced by an air volume and detector in water, Monte Carlo (MC) simulations were utilized to score the dose in water, in air volume in water and in complete model of LAC detector in water. Measurements were compared to MC calculations and some general properties of $DAPR_{20,10}$ in water were investigated. The aim of this study was to determine the features of $DAPR_{20,10}$ in cone-collimated small fields used in small-beam RT with MC calculations and the measurement feasibility of $DAPR_{20,10}$ and DAP with two commercial LAC detectors, film and diode detector.

Methods

Measurements

DAP and $DAPR_{20,10}$ measurements with LACs, film dosimetry and a diode were studied in small RT beams collimated with conical shape collimators (Brainlab AG, Munich, Germany) of 4, 7.5, 10, 20, 30 and 40 mm in diameter. Measurements were performed with 6 MV photon beam from Varian Clinac iX (Varian Medical Systems, Inc., Palo Alto, CA, USA) medical linear accelerator. The MC models of treatment head and beam were validated for the same unit. $DAPR_{20,10}$ is the ratio of the DAP at 20 cm depth with source-to-surface-distance (SSD) of 80 cm and the DAP at 10 cm depth with SSD of 90 cm, similarly to the definition of $TPR_{20,10}$. The $DAPR_{20,10}$ with LAC and diode measurements were determined and compared to MC calculations. DAPs from diode and film measurements were calculated as the dose integrals over the sensitive surface of the LACs as:

$$DAP = 2\pi \int_0^R g(r) r dr, \quad (1)$$

where R is the radius of the integrated dose or the active volume of the LAC, r is off-axis distance from beam center and $g(r)$ is dose profile. In this study and other publications (Djouguela *et al* 2006, Dufreneix *et al* 2016, Sánchez-Doblado *et al* 2007) the DAP is defined as the absorbed dose in an area of interest multiplied by this area of interest, which in LAC measurements is determined by the boundaries or the active area of the LAC. This should not be confused to the definition commonly used in diagnostic radiology, where the DAP is defined as the absorbed dose multiplied by the area of the radiation field rather than the measuring area of the IC itself.

LAC dosimetry

Two LACs, namely Bragg Peak chamber Type 34070 (PTW.70) and Type 34073 (PTW.73) manufactured by PTW (PTW-Freiburg GmbH, Freiburg, Germany) were studied (figure 1). They are vented and waterproof ionisation chambers (IC) originally designed for relative depth dose measurements in narrow proton and heavy ion beams. They have a similar but narrower guard ring as the plane parallel ICs used in clinical electron beam dosimetry. Both ICs consist of air volume with thickness of 2 mm. PTW.70 with detector diameter of 104 mm has an entrance window consisting of 0.10 mm lacquer, 3.35 mm polymethyl methacrylate (PMMA) and 0.02 mm graphite, which corresponds to 4.0 mm water-equivalent thickness for 6 MV photons. The diameters of the air volume and the active volume are 84.0 mm and 81.6 mm, respectively. PTW.73 with detector diameter of 68.0 mm has an entrance window consisting of 0.10 mm lacquer, 1.01 mm PMMA and 0.02 mm graphite, which corresponds to 1.29 mm water-equivalent thickness. The diameters of the air volume and the active volume are 48.0 mm and 39.6 mm, respectively. For both LACs the effective point of measurement was selected to be at the inner

surface of the entrance window. While the nominal bias voltage is +400 V, in this study, smaller and opposite polarity voltage of -250 V was used in order to diminish the polarity effect. PTW Semiflex chamber type 31010 (PTW-Freiburg GmbH, Freiburg, Germany) with active volume of 0.125 cm^3 was used as a reference detector in percentage depth dose-area product (PDDAP) measurement with the LACs for field sizes larger or equal to 20 mm in diameter. For the field sizes less than 20 mm in diameter, measurements were performed without the reference chamber in order to avoid the perturbations induced by it. The measured charge values were corrected for ambient conditions and recombination effects. The recombination correction was determined with the IAEA TRS-398 two-voltage method (IAEA Vienna 2000). The accuracy of this method was regarded sufficient for the relative $DAPR_{20,10}$ measurements.

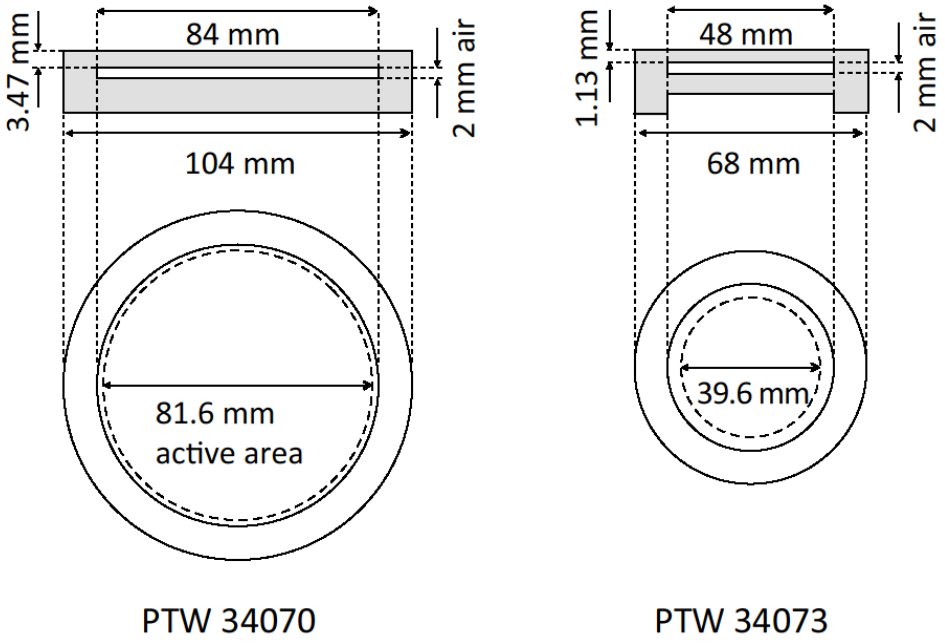

Figure 1. Diagrams of two different LACs. The diameters of the active volumes and the thicknesses of the entrance window are different. PTW.70 has an entrance window thickness of 3.47 mm, equivalent to 4.00 mm of water. PTW.73 has an entrance window thickness of 1.13 mm, equivalent to 1.29 mm of water (figure not to scale).

Film dosimetry

For relative off-axis dosimetry Gafchromic EBT3 (Ashland Inc., Wayne, NJ, USA) radiochromic film was used in a solid water RMI (Gammex Inc., WI, USA) phantom (Tello *et al* 1995). EBT3 film is self-developing so that there is no need for any additional processing (Dreindl *et al* 2014). For each field size, four films were irradiated at two different dose levels in order to achieve an optimal film dose response inside and outside the beam. Two films with the size of 10 cm x 20 cm were irradiated to 2 Gy dose for the evaluation of beam profile from 100% dose at the center to 50% dose at the penumbra and two films

to 20 Gy dose level at the beam center for the evaluation of beam profile from 50% dose level beyond. This enabled an increase in the accuracy of the low dose region profile evaluation. In this work the film calibration was valid only up to 10 Gy dose level. Films were scanned with a flatbed scanner (Epson Perfection V750-M Pro, Seiko Epson Corporation, Tokyo, Japan) using 72 dpi resolution corresponding to 0.3 x 0.3 mm^2 pixel size using the method described by Sipilä *et al* 2016.

Point measurements

For percentage depth dose (PDD), off-axis ratios (OAR) and $TPR_{20,10}$ measurements IBA Razor diode detector (IBA Dosimetry GmbH, Schwarzenburg, Germany) with sensitive volume of 0.006 mm^3 (diameter of 0.6 mm and thickness of 0.02 mm) was used. The OARs in lateral and longitudinal direction were averaged and dose integral was calculated and compared with film measurements and MC calculation results.

Monte Carlo calculations

The MC calculations were performed with the EGSnrc (v2016) code package (Kawrakow *et al* 2016). The geometry model of the Varian Clinac iX has been modelled with BEAMnrc user code (Ojala *et al* 2010, Ojala *et al* 2014a, Ojala *et al* 2014b and Ojala *et al* 2014c). To investigate the influence of the detector on the DAP, the MC-calculated DAP values in water, in air cavities and in active volumes of complete LAC models were modelled as is presented in figure 2. Dose in water was calculated in thin slabs of 0.2 mm thickness centered at 10 and 20 cm depths and SSDs of 90 and 80 cm, respectively. The radii of the slabs corresponded to the radii of the active volumes of the LACs. Air volumes in water corresponded to the air volumes in the LACs and the dose scoring volumes corresponded to the active volumes. Entrance surfaces of the air volumes were located at depths of 10 or 20 cm in water. Similarly, the complete LAC models with the entrance surfaces of the active volumes were set at depths of 10 or 20 cm in water. The authors received confidential detailed geometrical and material information from the manufacturer PTW-Freiburg. This information was used for the detector construction in the MC model. Particularly, the backwall material and electrodes were defined based on this information.

The phase space (phsp) files were generated with BEAMnrc for cone collimators of 4, 7.5, 10, 20, 30 and 40 mm in diameter at source distances of 80 and 90 cm. The phsp files were used as particle sources in the dose calculations in phantom with egs_chamber user code.

To investigate the $DAPR_{20,10}$ value as a function of integrated dose radius, the profiles were scored in water for the 7.5 mm cone at depths of 10 and 20 cm and SSDs of 90 and 80 cm, respectively. Ring thickness of 2.00 mm was used over the complete profile and width of 0.25 mm inside the field, 0.50 mm up to less than 10% OAR, 1.00 mm up to 30.00 mm off-axis and 2.00 mm up to 100.00 mm. All

rings were centered at the beam axis. The data were used to assess the suitability of Razor diode for profile measurements in water as well as film measurements in solid water for DAP evaluation. Dose calculations were performed using the following EGSnrc transport parameters: ECUT = 0.521 MeV, PCUT = 0.001 MeV, Global SMAX = $1x10^{10}$, ESTEPE = 0.25, XImax = 0.5, Skin depth for BCA = 3, Boundary crossing algorithm = EXACT, Electron-step algorithm = PRESTA-II, Spin effects = on, Brems angular sampling = KM, Brems cross sections = NIST, Photon cross sections = xcom, Electron Impact Ionization = On, Triplet production = On, Radiative Compton corrections = On, Bound Compton scattering = On, Pair angular sampling = KM, Pair cross sections = NRC, Photoelectron angular sampling = On, Rayleigh scattering = On, Atomic relaxations = On, Photonuclear attenuation = On. In order to improve the simulation efficiency the photon cross-section enhancement was turned on with an enhancement factor of 256.

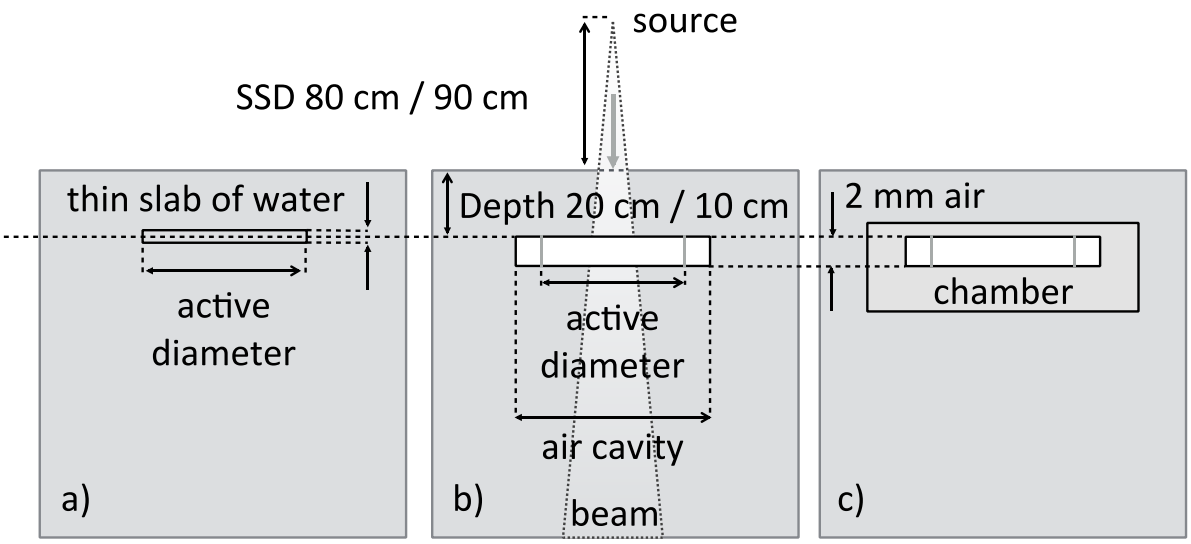

Figure 2. Geometries built in MC simulations to score the integral dose in volumes corresponding to active volumes of PTW.73 or PTW.70. Gray color represents water and white color represents air. Incident beam is drawn only in (b). In (a) the dose was scored in a thin 0.2-mm-thick slab of water with diameters of the active volumes of 39.6 mm or 81.6 mm, respectively. The water slab volume center is at 10 cm depth with SSD of 90 cm and at 20 cm depth with SSD of 80 cm. In (b) the air volume is that of the LAC air volume with thickness of 2.0 mm and diameters of 48.0 mm or 84.0 mm, respectively. The scoring volumes were again those of the active or measuring volumes of the LACs with diameters of 39.6 mm or 81.6 mm, respectively. The entrance surface of the air volume is at depth of 10 or 20 cm in water. In (c) the complete LACs were modelled with front and back wall electrodes and guard rings. The entrance surface of the air volume is at depth of 10 or 20 cm in water (MC = Monte Carlo; LAC = large-area chamber; SSD = source-to-surface distance).

Results

Figure 3(a) presents MC-calculated $DAPR_{20,10}$ values in water as a function of the integrated dose radius for 7.5 mm cone. From 10 to 50 mm radius of the dose integral, the increase in $DAPR_{20,10}$ is linear. From 50 up to 100 mm the increase is logarithmic. The linear part with a function $Ax + B$ was fitted with coefficient results of $A = 1.318 \cdot 10^{-3}$ and $B = 0.615$. The logarithmic part with a function $CLog_{10}(Dx) + E$ was fitted with coefficient results of $C = 0.146$, $D = 0.100$ and $E = 0.578$. In addition, calculated $DAPR_{20,10}$ values in two complete LAC detectors among measured values are plotted. As can be seen, the measured $DAPR_{20,10}$ values agree with MC calculations within one standard error. The measured $TPR_{20,10}$ values with Razor diode was added to the figure in order to be able to compare the $DAPR_{20,10}$ and $TPR_{20,10}$ values.

Figure 3(b) presents MC-calculated OARs at 20 and 10 cm depths and SSDs of 80 and 90 cm, respectively, together with the ratio OAR(d=20cm) / OAR(d=10cm). The OARs are normalized to beam CAX at 10 cm depth and SSD of 90 cm. For comparison to OAR(d=10cm), additional OAR(d=20cm) normalized to 100% at beam CAX at 20 cm depth is plotted. The overall average and maximum relative statistical uncertainties of the scored voxel doses to calculate OARs and $DAPR_{20,10}$ values in figure 3 were 0.12% and 0.26%, respectively.

As can be seen in figure 4, the $DAPR_{20,10}$ is larger for the larger LAC (PTW.70) for all studied cone sizes. For both LAC sizes, the $DAPR_{20,10}$ increases for field sizes less than 20 mm with photon nominal energy of 6 MV. There are small differences in $DAPR_{20,10}$ evaluated in air volume and water volume as can be seen in figures 3 and 4 and table 1 with maximum difference of 0.6%. The same is evident for the differences in $DAPR_{20,10}$ for detector and water with maximum difference of 0.8% evaluated by MC calculation. The overall average and maximum relative statistical uncertainties of the scored voxel doses to calculate $DAPR_{20,10}$ values in figure 4 were 0.08% and 0.17%, respectively.

MC-calculated $DAPR_{20,10}$ values differed maximally by 2.1% when compared to the measured ones, as is shown in table 2. On average, for PTW.73, calculations provided 1.1% greater DAP ratios when compared to measurements for the cones from 7.5 to 30 mm and 0.4% for the 4 mm cone, respectively. For PTW.70, the calculations agreed with the measurements with 0.1% maximum deviation for the cone sizes from 10 to 40 mm. For the 4 and 7.5 mm cones the differences were -2.1% and -0.9%, respectively.

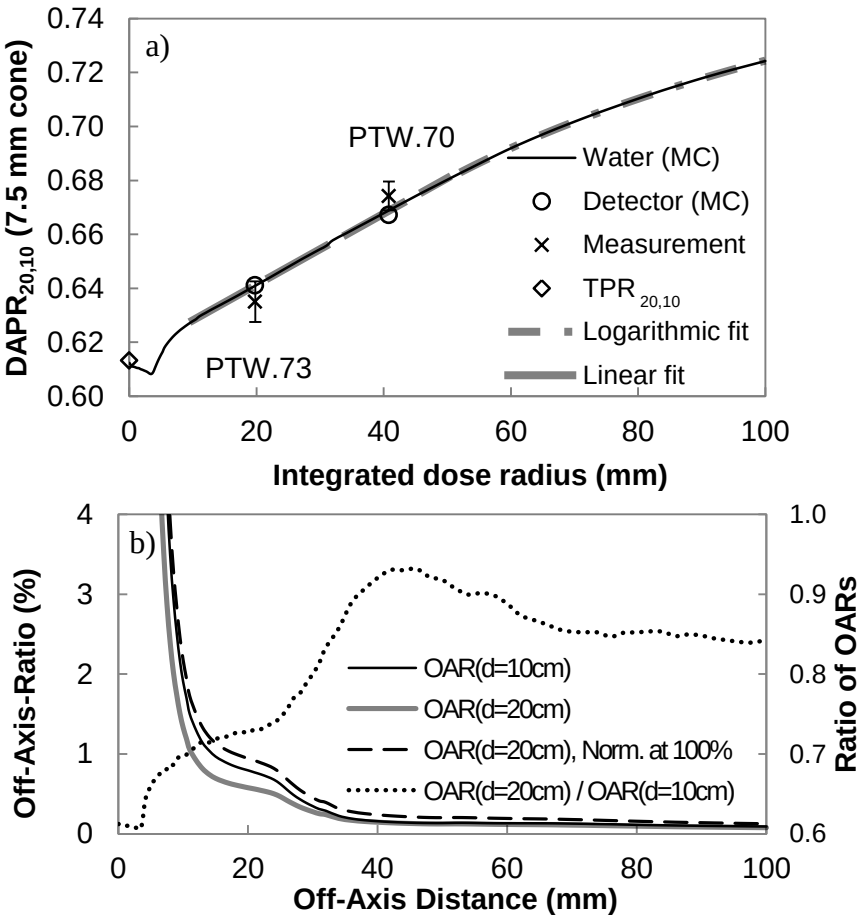

Figure 3. $DAPR_{20,10}$ as a function of integrated dose radius (a) and MC-calculated OARs at 20 and 10 cm depths and SSDs of 80 and 90 cm, respectively, together with the ratio of OARs (b) for 7.5 mm cone collimator. In a) MC-calculated $DAPR_{20,10}$ values are given in water (solid line) and in detector active volume (circle) together with LAC measurements (cross) and measurement error (1 σ). One standard deviation in MC-calculated ratios is 0.001 and is smaller than the symbol. Linear fit from 10 to 50 mm and logarithmic fit from 50 to 100 mm for $DAPR_{20,10}$ in water are plotted. For comparison, the measured $TPR_{20,10}$ value with Razor diode is added. In b) both OARs are normalized to 100% at CAX of the beam at 10 cm depth and SSD90. Ratio of OARs at 20 and 10 cm depths is plotted. For comparison, OAR at 20 cm depth normalized to 100% at beam CAX at 20 cm depth and SSD of 80 cm is added ($DAPR_{20,10}$ = dose-area product ratio at 20 and 10 cm depth; $TPR_{20,10}$ = tissue-phantom ratio at 20 and 10 cm depth; MC = Monte Carlo; LAC = large-area chamber; OAR = off-axis ratio; SSD = source-to-surface distance; CAX = center-of-axis).

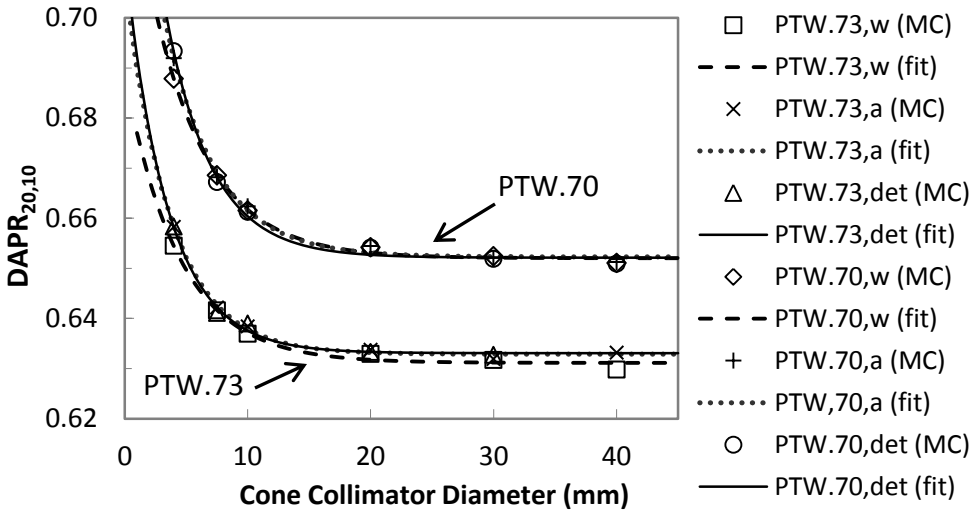

Figure 4. MC-calculated $DAPR_{20,10}$ corresponding to the LAC detectors PTW.73 and PTW.70 in a thin water (w) slab, in the active air (a) volumes and in the active air volumes of the LAC detectors (det). Fitted functions of the form $C \cdot exp(-Ax + B) + D$ are plotted (MC = Monte Carlo; $DAPR_{20,10}$ = dose-area product ratio at 20 and 10 cm depth; LAC = large-area chamber).

Table 1. MC-calculated $DAPR_{20,10}$ ratios of "air to water" and "detector to water".

		Cone collimator diameter (mm)						
Ratio	Chamber	4	7.5	10	20	30	40	Avg.
DAPR(20,10)air/	PTW.73	1.006	1.001	1.002	1.001	1.000	1.005	1.003
DAPR(20,10)w	PTW.70	1.006	0.999	1.001	1.000	1.000	1.000	1.001
DAPR(20,10)det/	PTW.73	1.006	0.999	1.003	1.001	1.002	-	1.002
DAPR(20,10)w	PTW.70	1.008	0.998	1.000	1.000	0.999	1.000	1.001

Table 2. Measured and calculated $DAPR_{20,10}$ and their relative difference for the two LACs PTW.73 and PTW.70. Overall, the calculated DAP ratios agree with measurements having a maximum relative difference of -2.1%. One standard deviation is shown in parentheses.

		Cone collimator diameter (mm)					
Chamber	Type	4	7.5	10	20	30	40
PTW.73	Meas.	0.656(7)	0.635(8)	0.632(7)	0.626(7)	0.626(7)	-
PTW.73	MC	0.658(1)	0.641(1)	0.639(1)	0.633(0)	0.633(0)	-
MC to meas.	Diff. (%)	0.41	0.95	1.16	1.18	1.10	-
PTW.70	Meas.	0.702(5)	0.674(5)	0.663(5)	0.655(5)	0.651(5)	0.651(5)
PTW.70	MC	0.687(1)	0.668(1)	0.662(0)	0.655(0)	0.652(0)	0.651(0)
MC to meas.	Diff. (%)	-2.10	-0.85	-0.10	-0.01	0.18	0.02

The smaller chamber PTW.73 was tested as a transmission reference chamber in depth dose and off-axis profile measurements with the IBA Razor diode, and the results were compared to those without

the reference chamber. Figure 5 demonstrates the measured depth dose and off-axis profiles for the 7.5 mm cone collimator at SSD of 90 cm with the off-axis profiles at 10 cm depth. For the depth dose, the largest difference of 0.8% is seen at 90 mm depth, and an average difference between reference chamber and non-reference condition is 0.2%. Calculated $PDD_{20,10}$ for both depth doses was 0.518. For off-axis profiles two orthogonal profiles in x- and y –directions were measured and an average was calculated. The largest deviation is seen at the penumbra region with -3.6% difference at 4.0 mm off-axis and the maximum distance to agreement is 0.09 mm. In regions of low dose gradient the dose deviations are less than 0.5%. The full-width at half-maximum (FWHM) of the off-axis profiles were 7.61 and 7.68 mm with and without the transmission reference IC, respectively.

In this work also the possibility of evaluating the DAP with point detector off-axis measurements in water and film measurements in solid water phantom were studied. Off-axis profiles are plotted in figures 6(a) and 6(b) for the 7.5-mm-cone together with Razor diode and EBT3 film measurements and the MC calculation. In addition, Farmer IC measurements at two points at out-of-field locations (cross) were added to figure 6(b). From these normalized profiles (100 % at CAX), the DAP was integrated according to equation (1) and plotted in figure 6(c).

The $DAPR_{20,10}$ values obtained with Razor diode measurements from profiles at 80 cm and 90 cm SSDs and at 20 cm and 10 cm depths, respectively, were compared to those of LAC measurements and the results are tabulated in table 3. The maximum relative differences of 0.7% and -0.9% and mean differences of 0.5% and -0.6% were found for PTW.73 and PTW.70, respectively. Overall mean difference was found to be -0.1%.

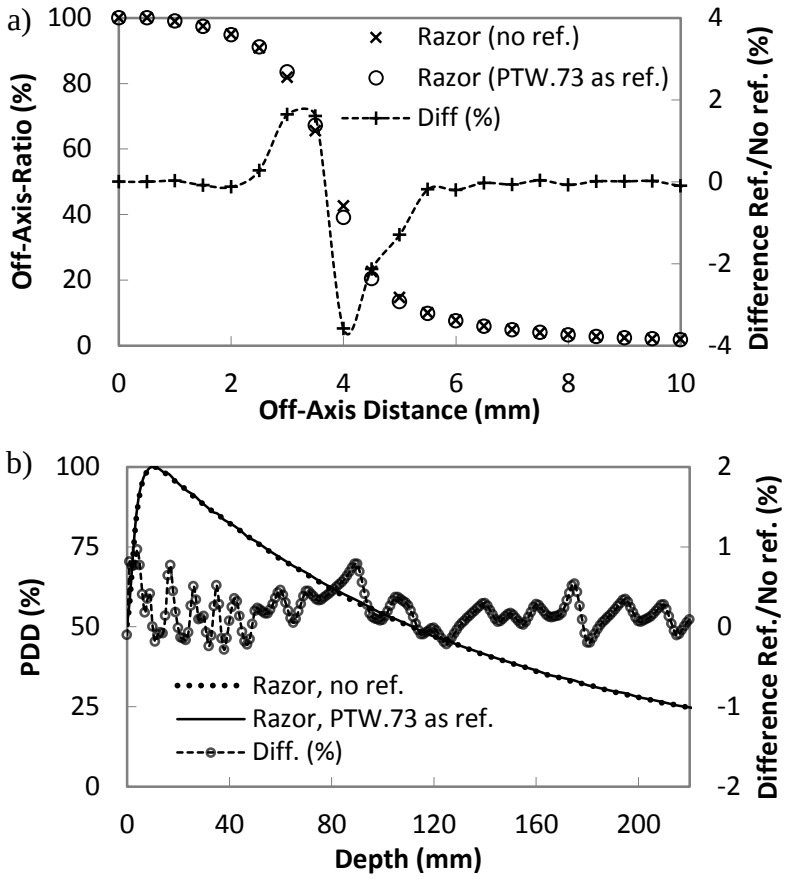

Figure 5. Measured off-axis profiles (a) and percentage depth dose (b) with and without the smaller LAC (PTW.73) as a reference chamber for the 7.5 mm cone. Off-axis profile is measured at 10 cm depth with SSD of 90 cm (PDD = percentage depth dose; LAC = large-area chamber).

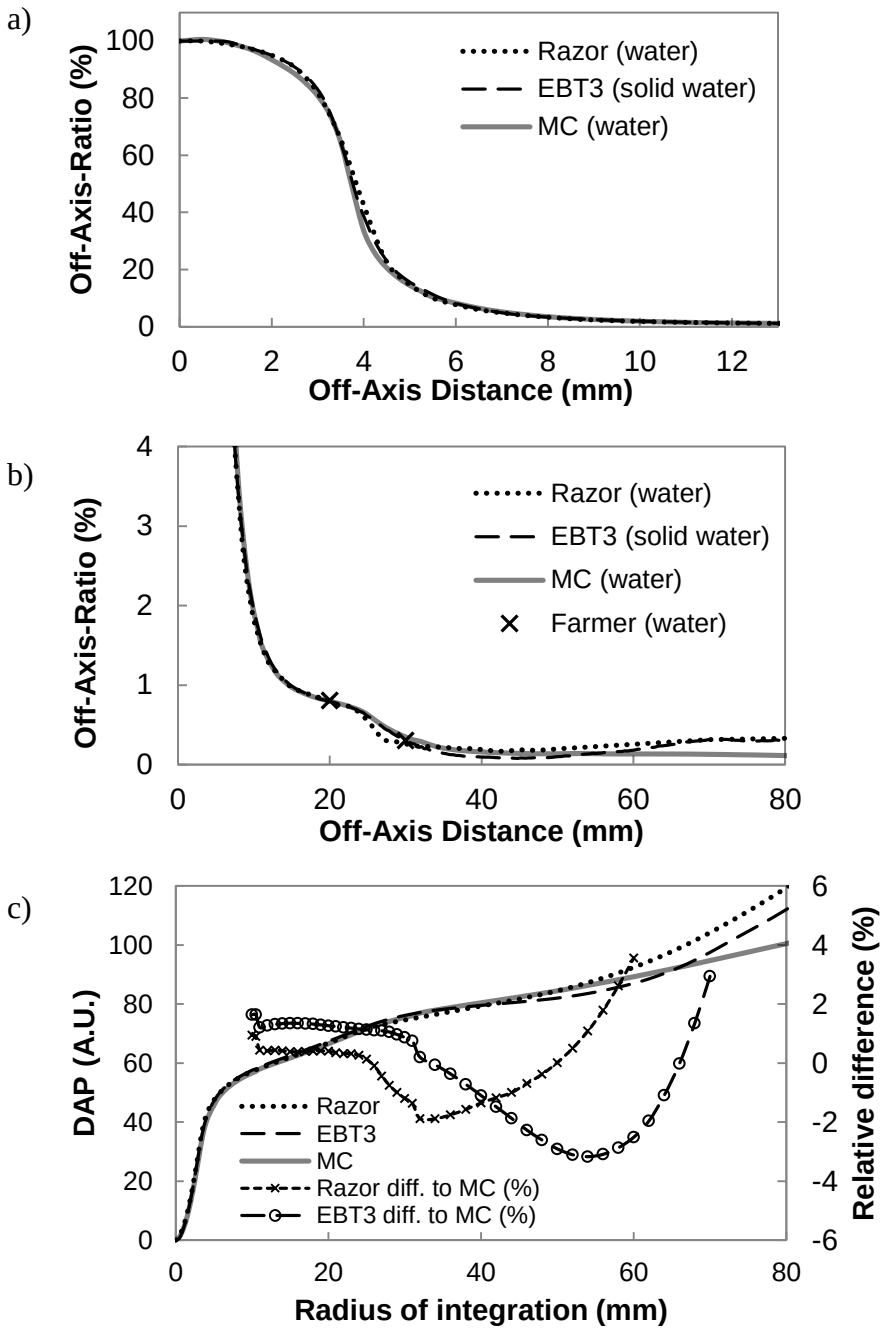

Figure 6. Measured and calculated central-axis normalized profiles of the 7.5 mm diameter cone collimator at depth of 10 cm and SSD of 90 cm (a and b). Razor diode and Farmer IC measurements and MC calculations are done in water and EBT3 film measurements in solid water. DAP is integrated from the profiles (a and b) obtained by Razor and EBT3 measurements and MC calculation (c) (MC = Monte Carlo; DAP = dose-area product; A.U. = arbitrary unit; SSD = source-to-surface distance).

Table 3. Comparison of the $DAPR_{20,10}$ values measured by LAC and Razor diode.

	Cone collimator diameter (mm)		
Detector	7.5	20	40
PTW.73	0.635	0.626	-
Razor	0.637	0.630	-
Difference (%)	0.31	0.66	-
PTW.70	0.674	0.655	0.651
Razor	0.668	0.652	0.648
Difference (%)	-0.89	-0.46	-0.46

The DAP ratio at 20 cm and 10 cm depths with a constant SSD of 90 cm was also determined with both LACs. To make a difference to the definition of $DAPR_{20,10}$, let us denote this as a percentage depth-dose-area-product ratio at 20 cm and 10 cm depths ($PDDAPR(SSD90)_{20,10}$). The $PDDAPR(SSD90)_{20,10}$ was evaluated for the smaller LAC with cone sizes of 4, 10, 20 and 30 mm and for the larger LAC with cone sizes of 4, 7.5, 10, 20, 40 mm. The results are shown in table 4 together with the $DAPR_{20,10}$ for comparison.

Table 4. Comparison of $PDDAPR(SSD90)_{20,10}$ and $DAPR_{20,10}$.

		Cone collimator diameter (mm)					
Chamber	Value	4	7.5	10	20	30	40
PTW.73	PDDAPR	0.612	-	0.621	0.622	0.615	-
PTW.73	DAPR	0.656	0.635	0.632	0.626	0.626	-
PTW.70	PDDAPR	0.660	0.652	0.652	0.647	-	0.646
PTW.70	DAPR	0.702	0.674	0.663	0.655	0.651	0.651

Discussion

MC calculations of DAP at 10 and 20 cm depths in water show that $DAPR_{20,10}$ increases with increasing integrated dose area after FWHM of the field (figure 3a) for 7.5 mm cone-collimated 6 MV photon field. There is no earlier publication in the literature describing this relationship, but the $DAPR_{20,10}$ results may be compared to the results in the study by Dufreneix *et al* 2016, who have evaluated the $DAPR_{20,10}$ for their own LAC in a 6 MV beam from Saturn 43 linear accelerator. For the cone-shape field diameters of 7.5, 10 and 20 mm they found a fairly constant $DAPR_{20,10}$ values of 0.645, 0.644 and 0.644, respectively. These results fall in between the results of this study, as can be seen in table 2. Based on the calculations and measurements it can be concluded that the $DAPR_{20,10}$ has a field size dependence with the field diameters less than 20 mm in the beam used in this study, but in addition it has a LAC size dependence.

The LAC that Dufreneix *et al* 2016 have used is 3 cm in diameter, which is smaller than both of the LACs used in this study. This means that the $DAPR_{20,10}$ value measured with a 3-cm-diameter LAC for 7.5-mm-cone beam used in this study should result in $DAPR_{20,10}$ value less than 0.635 according to the measurement with PTW.73 and approximately equal to 0.635 according to the calculation in water (figure 3a). This deviation of about 1.4% could be due to differences in beam collimation and quality, as well as differences in LAC construction. The increase in $DAPR_{20,10}$ with the increase of integration area is due to the larger contribution of low energy scattered photons at 20 cm depth of water, as compared to 10 cm depth, and this contribution ratio increases with the radius of dose integral as seen in figure 3(b). Indeed, the ratio of OARs increases with increasing radius after the penumbra. To emphasize this effect the OAR at 20 cm depth normalized to 100% at CAX is plotted. As can be seen, the relative out-of-field dose is greater at 20 than 10 cm depth. Thus, the larger is the LAC, the larger is the $DAPR_{20,10}$. On average, the $DAPR_{20,10}$ for the larger LAC was 5.2% and 3.7% larger than that of the smaller LAC according to the measurements and MC calculations, respectively (table 2). These findings refer to the fact that $DAPR_{20,10}$ values cannot be expressed only with regard to the beam properties but also to the integration area or size of the used LAC. This means that with reported $DAPR_{20,10}$ value there should be a reference to the size of the LAC active area or to the dose integral area. The largest relative differences of 6.8% and 4.3% between larger and smaller LAC were in the smallest field size of 4 mm diameter according to measurements and MC calculations, respectively. There was also greater field size dependence with larger integrated area. From 20 mm down to 4 mm field size the measurements indicate that $DAPR_{20,10}$ increases 4.7% for PTW.73 when compared to a 7.0% increase for PTW.70. On the other hand, from 20 to 40 mm field size the drop in $DAPR_{20,10}$ is 0.6% for the larger LAC and from 20 to 30 mm the field size stays constant for the smaller LAC suggesting that the $DAPR_{20,10}$ is fairly constant for field sizes equal or greater than 20 mm in diameter. The contributing factors to the increase of $DAPR_{20,10}$ value for the cone sizes less than 20 mm in diameter should be more closely investigated with MC calculations. However, it is evident that in the beam used in this study the relative out-of-field contribution to DAP is greater for cones less than 20 mm in diameter compared to cones greater than 20 mm. This means that the DAP values and thus the DAP ratio increases more rapidly with increasing integration area for the smaller cones. The increased cone collimator scatter of the smaller cones, source occlusion, lateral electron disequilibrium and even accelerator head radiation leakage might all contribute to this effect.

Small differences in $DAPR_{20,10}$ evaluated in air volume and water volume (figures 3 and 4, as well as table 1) with maximum relative difference of 0.6% shows that the air volume in water does not have a large effect on the $DAPR_{20,10}$ when compared to water volumes evaluated by MC calculation. The same thing is evident for the differences in $DAPR_{20,10}$ for detector and water with maximum relative

difference of 0.8%. It can be concluded that the air volume has approximately the same amount of perturbation contribution to the $DAPR_{20,10}$ value than that of the surrounding LAC material.

The $DAPR_{20,10}$ values were measured with two LAC detectors and compared to MC calculations. There is a calculation-to-measurement maximum relative difference of -2.1% and mean difference of -0.6% for the PTW.70 and those of +1.2% and +1.0% for the PTW.73, respectively. These differences may arise from uncertainties in measurements and in LAC models. The two-voltage method showed a drop of maximum 0.07% for recombination coefficient from 10 to 20 cm depth, which has a negligible effect to the DAP ratio. In the $DAPR_{20,10}$ determination 1 mm deviation at either depth results in about 0.5% error. Thus, one has to be careful when adjusting the depth of the LAC.

The $DAPR_{20,10}$ was evaluated by MC calculations using only PMMA as a backwall material for the PTW.73 chamber. In comparison to full geometry model, it has an impact on the DAP results with a maximum difference of -0.5% for the smallest field size of 4 mm at 20 cm depth. Mean differences of 0.0% and -0.2% at 10 and 20 cm depths for the field sizes of 4, 10 and 20 mm were found, respectively. For the $DAPR_{20,10}$ evaluation the maximum relative difference is -0.4% again for the smallest field size, the mean difference being -0.2%.

The depth dose and off-axis profile measurements were compared by using PTW.73 as transmission reference IC to measurements without a reference IC. Measurements provided equal depth-dose data with $PDD_{20,10}$ of 0.518. This implies that there can be only a minor difference in beam quality or spectrum present between the beams with and without the transmission reference chamber. The determined FWHM field sizes of 7.61 and 7.68 mm for the 7.5 mm cone-shape field with and without the transmission reference IC, respectively, and the overall mean off-axis dose difference of -0.1% and the maximum distance to agreement of 0.09 mm suggest that the LAC IC PTW.73 may be used as a reference transmission IC. The amount of signal in LAC is sufficient even with the smallest field of 4 mm in diameter.

The effect of the accelerator jaw setting on off-axis profiles is visible in figure 6(b) at off-axis-distance of 25 mm that corresponds exactly to the jaw setting of 5x5 cm^2 field at isocenter. The effect was found to be similar in both measurements and MC calculations. Obtained DAP by Razor diode measurements is comparable to EBT3 measurement and MC calculation as can be seen in figure 6(c). From DAP values at 90 and 80 cm SSDs and at 10 and 20 cm depths the $DAPR_{20,10}$ obtained with Razor diode are in good agreement with those derived from LAC measurements for the field sizes of 7.5, 20 and 40 mm, as can be seen in table 3 with maximum relative difference of -0.9%.

It has been argued, that $DAPR_{20,10}$ is not dependent on field size. In the beam quality and energy used in this study, this is the case for field sizes larger than 20 mm in diameter. Our findings indicate a fairly constant $DAPR_{20,10}$ value for cone sizes of 20 mm, 30 mm and 40 mm with maximum relative

difference of 0.6% for PTW.70. On the other hand, from 20 mm down to 4 mm cone there is a relative increase of 4.8% and 7.9% in the $DAPR_{20,10}$ value for PTW.73 and PTW.70, respectively. Consequently in the cone-collimated 6 MV photon beam, constant $DAPR_{20,10}$ was not observed for cone sizes ranging from 4 to 20 mm in diameter.

It can be seen from the results in table 4 that the relative variation in $PDDAPR(SSD90)_{20,10}$ is smaller than that in $DAPR_{20,10}$ for the cone sizes used in this study. There is a maximum relative change of 1.1% and 4.7% for the smaller LAC, and 2.1% and 7.6% for the larger LAC in $PDDAPR(SSD90)_{20,10}$ and $DAPR_{20,10}$ values, respectively.

The $DAPR_{20,10}$ value is a feasible beam quality parameter and the measurement is similar to that of the $TPR_{20,10}$ parameter. With the known size of LAC, this has potential to increase the accuracy in beam quality determination because of the smaller uncertainty due to the detector's placement. Thus, an increased accuracy of determined absorbed dose in a patient would be expected in the use of small-beam RT.

Conclusion

In this study, the measurement of $DAPR_{20,10}$ was investigated with two large area plane parallel Bragg-peak chambers (PTW.73 and PTW.70) for small conical fields of 4 to 40 mm in diameter in 6 MV photon beam. The properties of the $DAPR_{20,10}$ were determined by MC calculations. Comparisons were performed between measured and calculated values of $DAPR_{20,10}$. The dependence of the $DAPR_{20,10}$ on field size as well as on integrated dose area was demonstrated for the beam used in this study. With the calculations, the $DAPR_{20,10}$ values were evaluated in water, in air volumes corresponding to air volumes of the LAC detectors and in air volumes of the LACs themselves.

The use of the smaller LAC chamber PTW.73 as a transmission reference IC was shown to be applicable in depth dose and profile measurements for a small conical field of 7.5 mm in diameter. Razor diode detector was shown to be applicable for DAP and $DAPR_{20,10}$ evaluations. However, the benefit of using a point detector in $DAPR_{20,10}$ determination may be argued, as the same type of positioning uncertainty is evident as in $TPR_{20,10}$ determination. The $PDDAPR(SSD90)_{20,10}$ value with constant SSD had less variation with field size than $DAPR_{20,10}$ with varying SSD for cone-collimated beams used in this study.

The clinical relevance to use $DAPR_{20,10}$ instead of $TPR_{20,10}$ in small-beam RT should be further evaluated by comparing the overall uncertainty of the calculated patient target dose using $DAPR_{20,10}$ and $TPR_{20,10}$ as a beam quality parameter. To our knowledge, this is the first study evaluating the DAP and $DAPR_{20,10}$ values both with measurements and MC calculations, and showing the dependence of

$DAPR_{20,10}$ on field and LAC size. Determination of optimal LAC size for use in varying beam sizes and energies in a search for a constant $DAPR_{20,10}$ would require additional simulations and measurements.

Acknowledgements

This work was partially funded by the Finnish Cultural Foundation, Varsinais-Suomi Regional fund (grant 85151291) and Turku University Foundation (grant 12212). The authors wish to thank Mr. Pekka Aalto from Yanmedi Oy (Helsinki, Finland) and PTW-Freiburg GmbH (Freiburg, Germany) for a detector loan, and PTW-Freiburg for the delivery of confidential geometry and material composition information for the large-area chambers PTW Type 30473 and PTW Type 30470.

References

Alfonso R *et al* 2008 A new formalism for reference dosimetry of small and nonstandard fields *Med. Phys.* **35** 5179–86

IAEA International Atomic Energy Agency, Absorbed Dose Determination in External Beam Radiotherapy: An International Code of Practice for Dosimetry Based on Standards of Absorbed Dose to Water, Technical Report Series No. 398 *IAEA Vienna* 2000

Benmakhlouf H, Sempau J and Andreo P 2014 Output correction factors for nine small field detectors in 6 MV radiation therapy photon beams: A PENELOPE Monte Carlo study *Med. Phys.* **41** (4) 041711

Charles P H, Cranmer-Sargison G, Thwaites D I, Crowe S B, Kairn T, Knight R T, Kenny J, Langton C M, and Trapp J V 2014 A practical and theoretical definition of very small field size for radiotherapy output factor measurements *Med. Phys.* **41** (4) 041707

Das I J, Ding G X, Ahnesjö A 2008 Small fields: Nonequilibrium radiation dosimetry *Med. Phys.* **35**, 206–215

Djouguela A, Harder D, Kollhoff R, Rühmann A, Willborn K C, Poppe B 2006 The dose-area product, a new parameter for the dosimetry of narrow photon beams *Z. Med. Phys.* **16** 217–227

Dreindl R, Georg D, and Stock M 2014 Radiochromic film dosimetry: Considerations on precision and accuracy for EBT2 and EBT3 type films *Z. Med. Phys.* **24** 153–163

Dufreneix S, Ostrowsky A, Le Roy M, Sommier L, Gouriou J, Delaunay F, Rapp B, Daures J and Bordy J-M 2016 Using a dose-area product for absolute measurements in small fields: a feasibility study *Phys. Med. Biol.* **61** 650–662

Kawrakow I, Mainegra-Hing E, Rogers D W O, Tessier F, Walters B R B 2016 The EGSnrc Code System: Monte Carlo Simulation of Electron and Photon Transport *National Research Council of Canada. Ottawa, Canada, Report PIRS-701*

Li X A, Soubra M, Szanto J, and Gerig L H 1995 Lateral electron equilibrium and electron contamination in measurements of headscatter factors using miniphantoms and brass caps *Med. Phys.* **22** 1167-70

Ojala J, Hyödynmaa S, Baran´czyk R, Góra E, Waligórski MP 2014a Performance of two commercial electron beam algorithms over regions close to the lung–mediastinum interface, against Monte Carlo simulation and point dosimetry in virtual and anthropomorphic phantoms. *Phy.s Med.* **30** 147–54

Ojala J, Hyödynmaa S, Pitkänen M 2010 BEAMnrc Monte Carlo modelling of linear accelerator using parallel computing grid – validation of a common, fixed geometry model for photon and electron beams. In: *Proceedings of XVIth ICCR*, Amsterdam, Netherlands pp 1-4

Ojala JJ, Kapanen MK, Hyödynmaa SJ, Wigren TK, Pitkänen MA 2014b Performance of dose calculation algorithms from three generations in lung SBRT: comparison with full Monte Carlo-based dose distributions. *J. Appl. Clin. Med. Phys.* **15** (2) 4662

Ojala J, Kapanen M, Sipilä P, Hyödynmaa S, Pitkänen M 2014c The accuracy of Acuros XB algorithm for radiation beams traversing a metallic hip implant – comparison with measurements and Monte Carlo calculations. *J. Appl. Clin. Med. Phys.* **15** (5) 4912

Sánchez-Doblado F, Hartmann G H, Pena J, Roselló J V, Russiello G, Gonzalez-Castaño D M 2007 A new method for output factor determination in MLC shaped narrow beams *Phys. Med.* **23** 58–66

Sipilä P, Ojala J, Kaijaluoto S, Jokelainen I, Kosunen A 2016 Gafchromic EBT3 film dosimetry in electron beams — energy dependence and improved film read-out *J. Appl. Clin. Med. Phys.* **17** (1) 5970

Tello V M, Taylor R C and Hanson W F 1995 How water equivalent are water-equivalent solid materials for output calibration of photon and electron beams? *Med. Phys.* **22** (7) 1177-89